

# Vacuum Energy Density for Massless Scalar Fields in Flat Homogeneous Spacetime Manifolds with Nontrivial Topology

P. M. Sutter\* and Tsunefumi Tanaka†

*Physics Department, California Polytechnic State University, San Luis Obispo, CA 93407*

## Abstract

Although the observed universe appears to be geometrically flat, it could have one of 18 global topologies. A constant-time slice of the spacetime manifold could be a torus, Möbius strip, Klein bottle, or others. This global topology of the universe imposes boundary conditions on quantum fields and affects the vacuum energy density via Casimir effect. In a spacetime with such a nontrivial topology, the vacuum energy density is shifted from its value in a simply-connected spacetime. In this paper, the vacuum expectation value of the stress-energy tensor for a massless scalar field is calculated in all 17 multiply-connected, flat and homogeneous spacetimes with different global topologies. It is found that the vacuum energy density is lowered relative to the Minkowski vacuum level in all spacetimes and that the stress-energy tensor becomes position-dependent in spacetimes that involve reflections and rotations.

PACS numbers: 04.20.Gz

Keywords: topology, casimir, cosmology

---

\*Electronic address: psutter2@uiuc.edu; *Present address:* Department of Physics, University of Illinois at Urbana-Champaign, 1110 West Green Street, Urbana, IL 61801-3080

†Electronic address: tt22@humboldt.edu; *Present address:* Department of Physics and Physical Science, Humboldt State University, 1 Harpst Street, Arcata, CA 95521

## I. INTRODUCTION

No known laws of physics can predict the global topology of spacetime. However, the global topology of the universe plays an important role in quantum field theory. The geometrically flat, homogeneous, and isotropic universe could have one of 18 possible spatial manifolds with different topologies. Only one of these, the Euclidean plane, is simply-connected. The other 17 are multiply-connected; that is, the spacetime contains multiple geodesics between two points that cannot be continuously deformed into one another.

If the observable part of the universe is greater in size than the greatest simply-connected domain of a spacetime manifold, then the global topology of the universe will be directly observable. There are currently two major efforts to observationally determine the cosmic topology: cosmic crystallography and searches for circles in the sky. Researchers in cosmic crystallography use a statistical approach; they examine the separations of random pairs of galaxies in the sky. If the universe is multiply-connected, certain distances will appear more frequently in a statistical distribution. This method cannot determine the exact topology. For example, it cannot distinguish between a Möbius strip and a 1-Torus with twice the circumference.

The second effort, the circles in the sky, assumes that the visible universe has expanded enough that the last scattering surface (LSS) has intersected itself. The intersections appear as matching circles embedded in opposite sides of the cosmic microwave background radiation (CMBR). Temperature variations along the matching circles should be identical. This technique has the benefit of being able to exactly determine the cosmic topology. As of yet, neither of these techniques has produced a positive result. The LSS may not have extended enough to intersect itself. Or, the cosmic topology may be observable but complex and difficult to detect in current observations of the CMBR or galactic distributions.

The global topology of the universe also has a more subtle influence on fields. In a spacetime with a periodic boundary condition imposed by topology, only certain modes of a quantum field are allowed. As a result, the values of locally measurable quantities, such as the vacuum energy density of the field, are shifted from the values in a simply connected spacetime manifold. This is called the topological Casimir effect. DeWitt, Hart, and Isham [1] have perviously studied the Casimir effect on the vacuum expectation value of the stress-energy tensor,  $\langle 0|T_{\mu\nu}|0\rangle$ , for massless scalar fields in several spacetimes with

nontrivial topology. In this paper we extend their work to all possible flat manifolds, including non-orientable manifolds. In Section II we outline the method of images to calculate  $\langle 0|T_{\mu\nu}|0\rangle$  for a free massless scalar field in a multiply-connected spacetime. We present the results of our calculations in Sections III through VII. Finally, we summarize the effects of multiple-connectedness, orientability, and other topological modifications on the vacuum energy density in Section VIII.

In this paper we assume that the universe is static, flat, and homogeneous. We will look at spacetime manifolds with the structure time  $(\mathbb{R}) \times$  space  $(\mathcal{M}_3)$  where  $\mathcal{M}_3$  is a three-dimensional spatial hypersurface having the Euclidean space  $\mathbb{R}^3$  as the universal covering space. By nontrivial topology of spacetime, we mean topology of the space  $\mathcal{M}_3$ , not the spacetime. Also, we will use natural units where  $G = \hbar = c = 1$ , and the metric signature of  $+2$ .

## II. THE STRESS-ENERGY TENSOR AND THE METHOD OF IMAGES

Calculation of the vacuum expectation value of the stress-energy tensor in a flat universe with nontrivial topology is relatively straightforward. This is due to the facts that all curvature components vanish in a flat geometry and that topology of the manifold appears only in an interval between two points in spacetime. Once the interval for a particular spacetime manifold is found, the calculation of  $\langle 0|T_{\mu\nu}|0\rangle$  reduces to simple differentiation of the Hadamard elementary function, taking the coincidence limit, and subtracting an appropriate infinity to renormalize its value.

The stress-energy tensor for a massless free scalar field  $\phi(x)$  is given by

$$T_{\mu\nu} = (1 - 2\xi)\phi_{;\mu}\phi_{;\nu} + \left(2\xi - \frac{1}{2}\right)g_{\mu\nu}\phi_{;\alpha}\phi^{;\alpha} - 2\xi\phi\phi_{;\mu\nu}, \quad (1)$$

where  $\xi$  is the curvature coupling constant. We will let  $\xi = \frac{1}{6}$  for conformal coupling. The scalar field satisfies the massless Klein-Gordon equation  $\square_x\phi(x) = 0$ .

Since every term in  $T_{\mu\nu}$  is quadratic in the field variable  $\phi$ , we can split the point  $x$  into the two points  $x$  and  $\tilde{x}$ , and after taking covariant derivatives of  $\phi$ , the two points are brought back together in the coincidence limit  $\tilde{x} \rightarrow x$ :

$$T_{\mu\nu} = \frac{1}{2} \lim_{\tilde{x} \rightarrow x} \left[ (1 - 2\xi)\nabla_\mu \tilde{\nabla}_\nu + \left(2\xi - \frac{1}{2}\right)g_{\mu\nu}\nabla_\alpha \tilde{\nabla}^\alpha - 2\xi\nabla_\mu \nabla_\nu \right] \{\phi(x), \phi(\tilde{x})\}. \quad (2)$$

Since there is no preference for either point, the stress-energy tensor  $T_{\mu\nu}$  is symmetrized over  $x$  and  $\tilde{x}$ . The covariant derivative  $\nabla_\mu$  and  $\tilde{\nabla}_\nu$  are to be applied to  $\phi(x)$  and  $\phi(\tilde{x})$ , respectively. The expectation value of the stress-energy tensor needs to be evaluated with respect to the vacuum state in each spacetime.

The Minkowski vacuum state, denoted by  $|0_M\rangle$ , is defined in terms of the positive frequency modes,

$$u_{\mathbf{k}} = \frac{e^{-ik_\alpha x^\alpha}}{[2\omega(2\pi)^3]^{\frac{1}{2}}}, \quad (3)$$

which are plane-wave solutions for the Klein-Gordon equation. The vacuum state is the state which is annihilated by the operator  $a_{\mathbf{k}}$  for all wave vectors  $\mathbf{k}$ :

$$a_{\mathbf{k}}|0_M\rangle = 0. \quad (4)$$

The spatial part of the Minkowski space is a three-dimensional Euclidean space, and thus there is no restriction for values of the wave vector  $\mathbf{k}$ .

If a boundary condition is imposed on the space, only a set of certain discrete modes will be allowed. For example, if the space is periodic in the  $x$  direction, then the  $x$ -component of  $\mathbf{k}$  will be allowed to have only values equal to  $2\pi n/L$ , where  $L$  is the circumference of the space in the  $x$  direction and  $n$  is any non-zero integer. This is because a plane wave travelling around the space in the closed direction will be out of phase with itself if its wavelength has a value other than  $L/n$ , and thus will destructively interfere with itself. Let  $\mathbf{k}_n$  be the allowed discrete mode. The vacuum state  $|0\rangle$  of this multiply-connected spacetime is defined by

$$a_{\mathbf{k}_n}|0\rangle = 0 \quad (5)$$

for all allowed values of  $\mathbf{k}_n$ . This vacuum state is different from the Minkowski vacuum state  $|0_M\rangle$ . Different boundary conditions on the space manifold will result in different vacuum states.

The vacuum expectation value of the stress-energy tensor can be written as

$$\langle 0|T_{\mu\nu}|0\rangle = \frac{1}{2} \lim_{\tilde{x} \rightarrow x} \left[ (1 - 2\xi) \nabla_\mu \tilde{\nabla}_\nu + \left( 2\xi - \frac{1}{2} \right) g_{\mu\nu} \nabla_\alpha \tilde{\nabla}^\alpha - 2\xi \nabla_\mu \nabla_\nu \right] D^{(1)}(x, \tilde{x}), \quad (6)$$

where the Hadamard elementary function for a massless scalar field,  $D^{(1)}(x, \tilde{x})$ , is defined as the vacuum expectation value of the anticommutator of the field variables:

$$D^{(1)}(x, \tilde{x}) \equiv \langle 0|\{\phi(x), \phi(\tilde{x})\}|0\rangle. \quad (7)$$

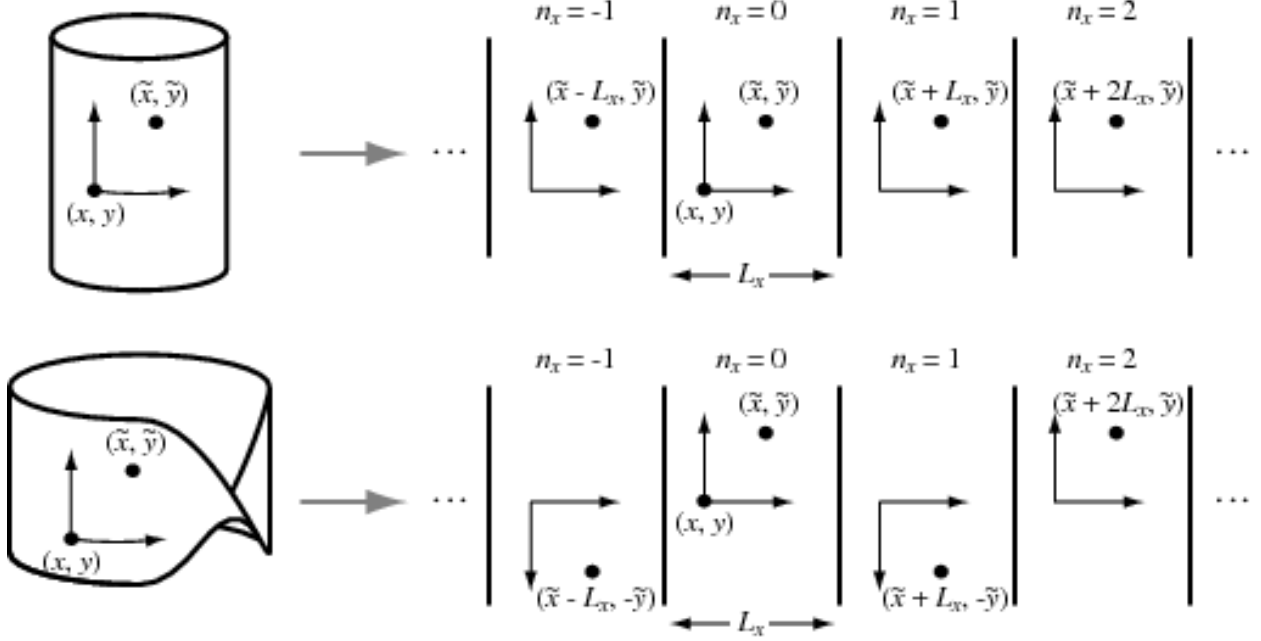


FIG. 1: Unrolling a cylinder (top) and Möbius Strip (bottom) to determine image point locations.

$D^{(1)}$  satisfies the massless Klein-Gordon equation  $\square_x D^{(1)}(x, \tilde{x}) = 0$ .

The vacuum stress-energy tensor as defined by Eq. (6) is infinite, and it must be renormalized by subtracting an appropriate infinity from it. The correct value to subtract is given by the normal ordering of the creation and annihilation operators, and it turns out to be the Minkowski vacuum expectation value. Thus, the renormalized vacuum expectation value of the stress-energy tensor in a spacetime with nontrivial topology is given by

$$\langle T_{\mu\nu} \rangle \equiv \langle 0|T_{\mu\nu}|0 \rangle_{ren} = \langle 0|T_{\mu\nu}|0 \rangle - \langle 0_M|T_{\mu\nu}|0_M \rangle. \quad (8)$$

Notice that the normalized stress-energy tensor in Minkowski space is identically zero.

The Hadamard function for a massless scalar field in Minkowski space is a simple function of the half-squared interval  $\sigma$  between two points  $x$  and  $\tilde{x}$ :

$$D^{(1)}(x, \tilde{x}) = \frac{1}{4\pi\sigma}, \quad (9)$$

where  $\sigma$  is defined as

$$\sigma = \frac{1}{2}[-(t - \tilde{t})^2 + (x - \tilde{x})^2 + (y - \tilde{y})^2 + (z - \tilde{z})^2].$$

The Hadamard function for a spacetime with nontrivial topology has the same functional form as the Minkowski case, but we replace  $\sigma$  in Eq. (9) to reflect the different periodic

boundary conditions of our chosen spacetime. Because the spacetime is multiply-connected, there can be more than one interval connecting two points  $(t, x, y, z)$  and  $(\tilde{t}, \tilde{x}, \tilde{y}, \tilde{z})$ . For example, suppose the spacetime is closed in the  $x$ -direction. We can connect  $(t, x, y, z)$  and  $(\tilde{t}, \tilde{x}, \tilde{y}, \tilde{z})$  with a direct path, or we can start from  $(t, x, y, z)$  and circle around in the  $x$ -direction once, twice, or an arbitrary number of times before arriving at  $(\tilde{t}, \tilde{x}, \tilde{y}, \tilde{z})$ . Since each path which wraps around cannot be deformed into another that wraps around a different number of times, we must take into account all nonequivalent paths by summing over them, from  $n = -\infty$  to  $n = \infty$ , where  $n$  would represent the number of loops around the space.

Equivalently, we can unwrap the space and tile copies of itself in a way required by the topology of the space. In each copy there is an image of the original point  $(\tilde{t}, \tilde{x}, \tilde{y}, \tilde{z})$ . A path connects  $(t, x, y, z)$  to each image of  $(\tilde{t}, \tilde{x}, \tilde{y}, \tilde{z})$ . The top of Figure 1 demonstrates this technique. The  $x$ -coordinates of the image points are  $\tilde{x} \pm L_x, \tilde{x} \pm 2L_x \dots, \tilde{x} \pm n_x L_x$ , where  $L_x$  is the circumference in the closed spatial direction. Thus, we define  $\sigma$  for for this space as

$$\sigma = \frac{1}{2}[-(t - \tilde{t})^2 + (x - \tilde{x} - n_x L_x)^2 + (y - \tilde{y})^2 + (z - \tilde{z})^2]. \quad (10)$$

We must sum over every contribution from each image point to construct the Hadamard function for a particular spacetime.

The term  $n_x = 0$  corresponds to the case with no boundary. This is the term which will give us an infinity associated with the unrenormalized stress-energy tensor of Minkowski space and will be subtracted in Eq. (8). So by excluding the  $n_x = 0$  term from the summation, the renormalized Hadamard function  $D_{ren}^{(1)}(x, \tilde{x})$  is obtained:

$$D_{ren}^{(1)}(x, \tilde{x}) = \sum'_{n_x} D^{(1)}(\sigma) \equiv \sum_{\substack{n_x = -\infty \\ n_x \neq 0}}^{\infty} D^{(1)}(\sigma), \quad (11)$$

where  $\Sigma'$  will indicate skipping over the simply-connected case. For intervals with multiple summation indices, this means skipping the case where all indices are simultaneously 0. Finally, using Eq. (6), the renormalized stress-energy tensor  $\langle T_{\mu\nu} \rangle$  can be defined as

$$\langle T_{\mu\nu} \rangle = \frac{1}{2} \lim_{\tilde{x} \rightarrow x} \left[ (1 - 2\xi) \nabla_\mu \tilde{\nabla}_\nu + \left( 2\xi - \frac{1}{2} \right) g_{\mu\nu} \nabla_\alpha \tilde{\nabla}^\alpha - 2\xi \nabla_\mu \nabla_\nu \right] D_{ren}^{(1)}(x, \tilde{x}). \quad (12)$$

The procedure for calculating  $\langle T_{\mu\nu} \rangle$  can be summarized as: (1) write an appropriate  $\sigma$  (i.e. determine the interval) for each manifold, (2) sum over the correct indices to construct

the renormalized Hadamard function, (3) apply the derivative operator in Eq. (12), and (4) take the coincidence limit as  $\tilde{x} \rightarrow x$ . A table of the spacetimes having the three-dimensional Euclidean space as a universal covering space and their properties can be found in [2]. We will investigate each of these spaces individually.

### III. ONE CLOSED DIMENSION

We begin by modifying the Euclidean 3-Space in the simplest possible way: closing one dimension to form a loop. This can be constructed by identifying a single pair of opposite faces of a rectangular box. The space's Fundamental Polyhedron (the most basic, simply-connected spatial domain that we can tile to create the universal covering space) is thus a "slab" of space, with a finite uniform thickness  $L_x$  in the  $x$ -direction, and infinite extension in the  $y$ - and  $z$ -directions. This space can also admit a flipping in one of the open dimensions, resulting in a Möbius Strip.

#### A. 1-Torus ( $E_{16}$ )

The half-squared interval  $\sigma$  of a simple 1-Torus is given by Eq. (10), where  $n_x$  is an integer. Inserting this interval into Eq. (9) and calculating the expectation value of the stress-energy tensor yields

$$\langle T_{\mu\nu} \rangle_{E_{16}} = \frac{\pi^2}{90L_x^4} \text{diag} [-1, -3, 1, 1]. \quad (13)$$

This result was originally obtained by DeWitt and others [1]. Note that the vacuum energy density  $\rho = \langle T_{00} \rangle_{E_{16}}$  is constant and less than zero throughout the space. As the circumference  $L_x$  of the space increases, the vacuum energy density approaches zero. For the calculation of  $\langle T_{\mu\nu} \rangle$  for a massive scalar field with an arbitrary curvature coupling in the 1-Torus Space, see Tanaka and Hiscock [3].

#### B. 1-Torus with Flip ( $E_{17}$ )

If we unroll a Möbius Strip onto a flat plane, we see as in the bottom of Figure 1 an interval of

$$\sigma = \frac{1}{2} \{ -(t - \tilde{t})^2 + (x - \tilde{x} - n_x L_x)^2 + [y - (-1)^{n_x} \tilde{y}]^2 + (z - \tilde{z})^2 \}^2. \quad (14)$$

Every time we slide by  $L_x$  in the  $x$  direction, the  $y$  coordinate of the image point changes its sign. This is the first of our non-orientable manifolds. Note that  $L_x$  is defined as the circumference of the universe, instead of the distance the field must traverse to return to the original state. In the latter view, the Fundamental Polyhedron is now of width  $2L_x$ . DeWitt, Hart, and Isham [1] have shown that the vacuum stress-energy tensor in the 1-Torus with Flip (designated as  $E_{17}$  in [2]) is

$$\langle T_{\mu\nu} \rangle_{E_{17}} = \frac{1}{16} \langle T_{\mu\nu} \rangle_{E_{16}} + \langle T_{\mu\nu} \rangle_{flip}(y), \quad (15)$$

where

$$\langle T_{\mu\nu} \rangle_{flip}(y) = \frac{2}{3\pi^2} \sum_{\substack{n_x \\ n_x \text{ odd}}} \frac{L_x^2 n_x^2}{(L_x^2 n_x^2 + 4y^2)^3} \cdot \text{diag}[-1, -2, 0, 1],$$

which can be written in terms of elementary functions:

$$\begin{aligned} \langle T_{\mu\nu} \rangle_{flip}(y) = & \frac{1}{192\pi L_x^3 y^3} \left\{ L_x^2 \tanh\left(\frac{\pi y}{L_x}\right) - \pi y \operatorname{sech}^2\left(\frac{\pi y}{L_x}\right) \left[ L_x - 2\pi y \tanh\left(\frac{\pi y}{L_x}\right) \right] \right\} \\ & \times \text{diag}[-1, -2, 0, 1]. \end{aligned}$$

Because the field must traverse the universe twice in the  $x$ -direction to have the same value, the circumference of the universe is effectively doubled, and the constant shift in the stress-energy is only 1/16 of that for the 1-Torus Space without flip. Also,  $\langle T_{\mu\nu} \rangle$  is now  $y$ -dependent (see Fig. 2).

#### IV. TWO CLOSED DIMENSIONS

Now, we close the space in two directions,  $x$  and  $y$ , but let it extend to infinity in the  $z$ -direction. The space is a stack of rectangular columns of depth  $L_x$ , width  $L_y$ , and infinite height in the  $z$ -direction. While stacking, four transformations can be introduced: horizontal flip, vertical flip, half-turn, and half-turn with flip. In these spaces, each  $z = \text{const}$  slice will be either a 2-Torus or a Klein bottle.

##### A. 2-Torus ( $E_{11}$ )

The half-squared interval of the simple 2-Torus is given by

$$\sigma = \frac{1}{2} [-(t - \tilde{t})^2 + (x - \tilde{x} - n_x L_x)^2 + (y - \tilde{y} - n_y L_y)^2 + (z - \tilde{z})^2]^2. \quad (16)$$



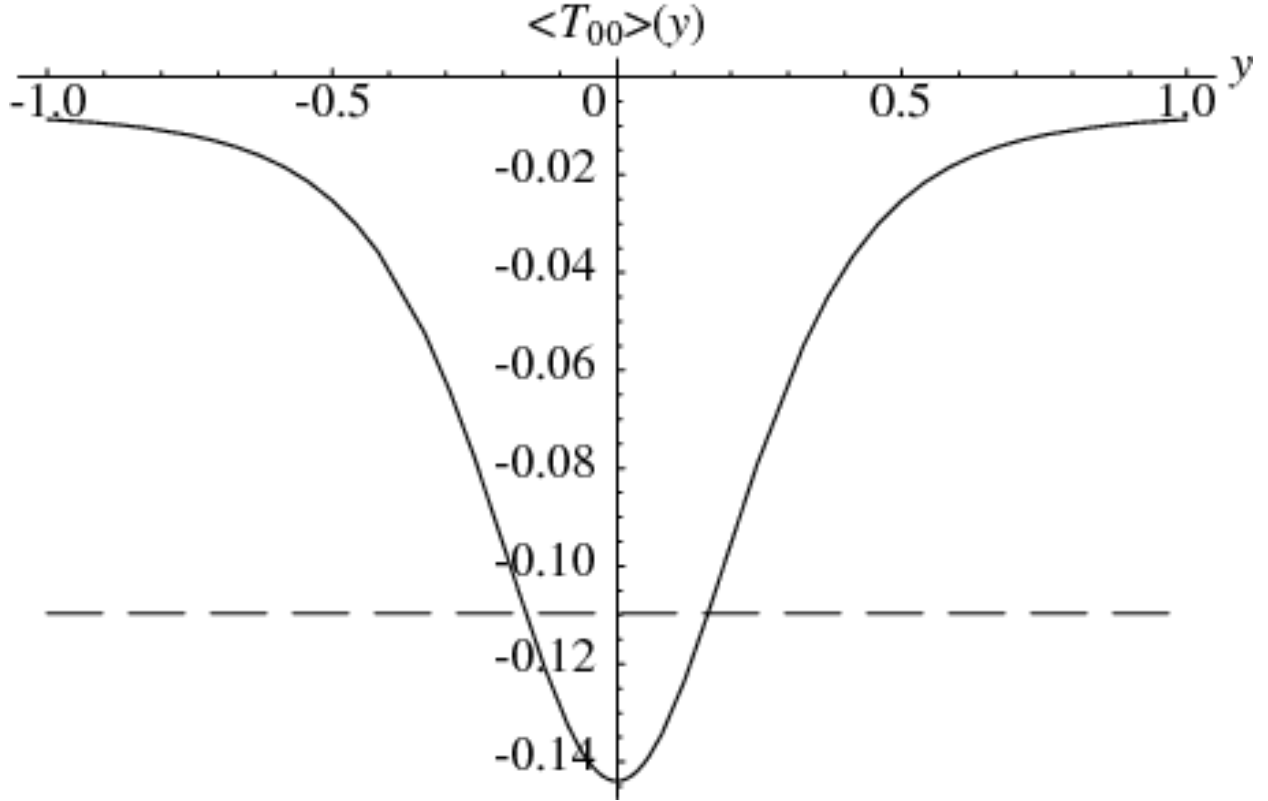


FIG. 2: The solid line is the vacuum energy density in 1-Torus with Flip. The dashed line indicates the constant energy density value for the 1-Torus. The  $y$ -axis extends to infinity in either direction.

The expectation value for this space is

$$\langle T_{\mu\nu} \rangle_{E_{11}} = \sum'_{n_x, n_y} [2\text{-Torus}], \quad (17)$$

where

$$[2\text{-Torus}] = \frac{1}{2\pi^2} \frac{1}{(L_x^2 n_x^2 + L_y^2 n_y^2)^3} \times (L_x^2 n_x^2 \text{diag}[-1, -3, 1, 1] + L_y^2 n_y^2 \text{diag}[-1, 1, -3, 1]). \quad (18)$$

Although this summation is not expressible in terms of elementary functions, it is convergent and results in a uniform negative shift in the vacuum energy level throughout the space.

### B. 2-Torus with Vertical Flip ( $E_{13}$ )

For this space, the vertical (non-closed) dimension,  $z$ , is flipped when gluing opposite faces in the  $x$ -direction. The interval for this space is

$$\sigma = \frac{1}{2} \{ -(t - \tilde{t})^2 + (x - \tilde{x} - n_x L_x)^2 + (y - \tilde{y} - n_y L_y)^2 + [z - (-1)^{n_x} \tilde{z}]^2 \}, \quad (19)$$

and the resulting stress-energy tensor has the form

$$\langle T_{\mu\nu} \rangle_{E_{13}} = \sum'_{n_x \text{ even}, n_y} [2\text{-Torus}] + \sum_{n_x \text{ odd}, n_y} [\text{V-Flip}(z)], \quad (20)$$

where

$$\begin{aligned} [\text{V-Flip}(z)] &= \frac{2}{3\pi^2} \frac{1}{(L_x^2 n_x^2 + L_y^2 n_y^2 + 4z^2)^3} \\ &\quad \times (L_x^2 n_x^2 \text{diag}[-1, -2, 1, 0] + L_y^2 n_y^2 \text{diag}[-1, 1, -2, 0]). \end{aligned}$$

The first summation corresponds to the stress-energy for the 2-Torus. This summation is exactly the same as the ordinary 2-Torus case if the interval in the  $x$ -direction is doubled. The  $z$ -dependence appears in the summation over odd values of  $n_x$ . Since  $z$  is not a closed dimension, the vacuum energy density is a single well that is most negative in the  $z = 0$  plane. The plot of the vacuum energy density is shown in Figure 3 (a).

### C. 2-Torus with Horizontal Flip ( $E_{14}$ )

As we translate in  $x$  we may instead choose to flip in the horizontal, or closed dimension,  $y$ . Then the interval becomes

$$\sigma = \frac{1}{2} \{ -(t - \tilde{t})^2 + (x - \tilde{x} - n_x L_x)^2 + [y - (-1)^{n_x} \tilde{y} - n_y L_y]^2 + (z - \tilde{z})^2 \}. \quad (21)$$

The vacuum stress-energy tensor is now

$$\langle T_{\mu\nu} \rangle_{E_{14}} = \sum'_{n_x \text{ even}, n_y} [2\text{-Torus}] + \sum_{n_x \text{ odd}, n_y} [\text{H-Flip}(y)], \quad (22)$$

with

$$[\text{H-Flip}(y)] = \frac{2}{3\pi^2} \frac{L_x^2 n_x^2}{[L_x^2 n_x^2 + (2y - L_y n_y)^2]^3} \text{diag}[-1, -2, 0, 1].$$

Since  $y$  is a closed dimension, a periodic energy density well appears in that direction (see Figure 3 (b)).

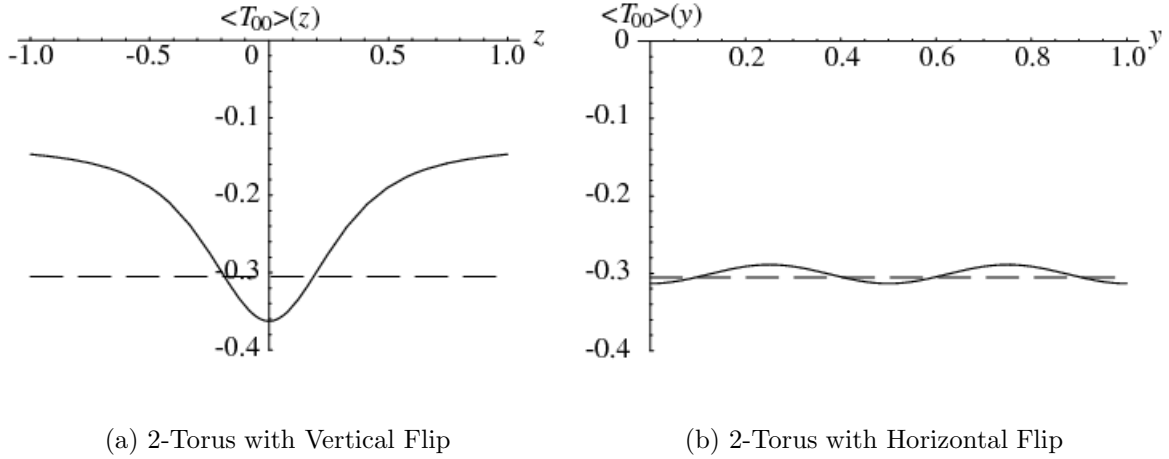


FIG. 3: Vacuum energy densities in the 2-Torus with Vertical and Horizontal Flips, with  $L_x = L_y = L_z = 1$ . The dashed line is the value for the plain 2-Torus. The regions are  $x = \text{const}$  slices of the Fundamental Polyhedra. The  $z$ -axis extends to infinity in either direction.

#### D. 2-Torus with Half-Turn ( $E_{12}$ )

The vertical and horizontal flip can be combined to generate a half-turn corkscrew motion when opposite faces in the  $x$ -direction are glued. Aside from the plain 2-Torus, this is the only orientable manifold with 2 closed dimensions. Combining the intervals of the two previous flips gives

$$\sigma = \frac{1}{2} \{ -(t - \tilde{t})^2 + (x - \tilde{x} - n_x L_x)^2 + [y - (-1)^{n_x} \tilde{y} - n_y L_y]^2 + [z - (-1)^{n_x} \tilde{z}]^2 \}. \quad (23)$$

The resulting expectation value is also a combination of the two flips:

$$\langle T_{\mu\nu} \rangle_{E_{12}} = \sum'_{n_x \text{ even}, n_y} [2\text{-Torus}] + \sum_{n_x \text{ odd}, n_y} [\text{Turn}(y, z)], \quad (24)$$

where

$$\begin{aligned} [\text{Turn}(y, z)] = & \frac{1}{6\pi^2} \frac{1}{[L_x^2 n_x^2 + (2y - L_y n_y)^2 + 4z^2]^3} \\ & \times \left\{ L_x^2 n_x^2 \text{diag}[-5, -7, 1, 1] + (2y - L_y n_y)^2 \text{diag}[-1, 1, 1, -3] \right. \\ & \left. + 4z^2 \text{diag}[-1, 1, -3, 1] - 8(2y - L_y n_y)z (\delta_\mu^y \delta_\nu^z + \delta_\mu^z \delta_\nu^y) \right\}. \end{aligned}$$

There are now non-zero off-diagonal terms in  $\langle T_{\mu\nu} \rangle$ . In fact, we find off-diagonal elements every time a space is rotated. As expected, we have periodic behavior in  $y$  and a single well in  $z$ . The energy density in this space is shown in Figure 4.

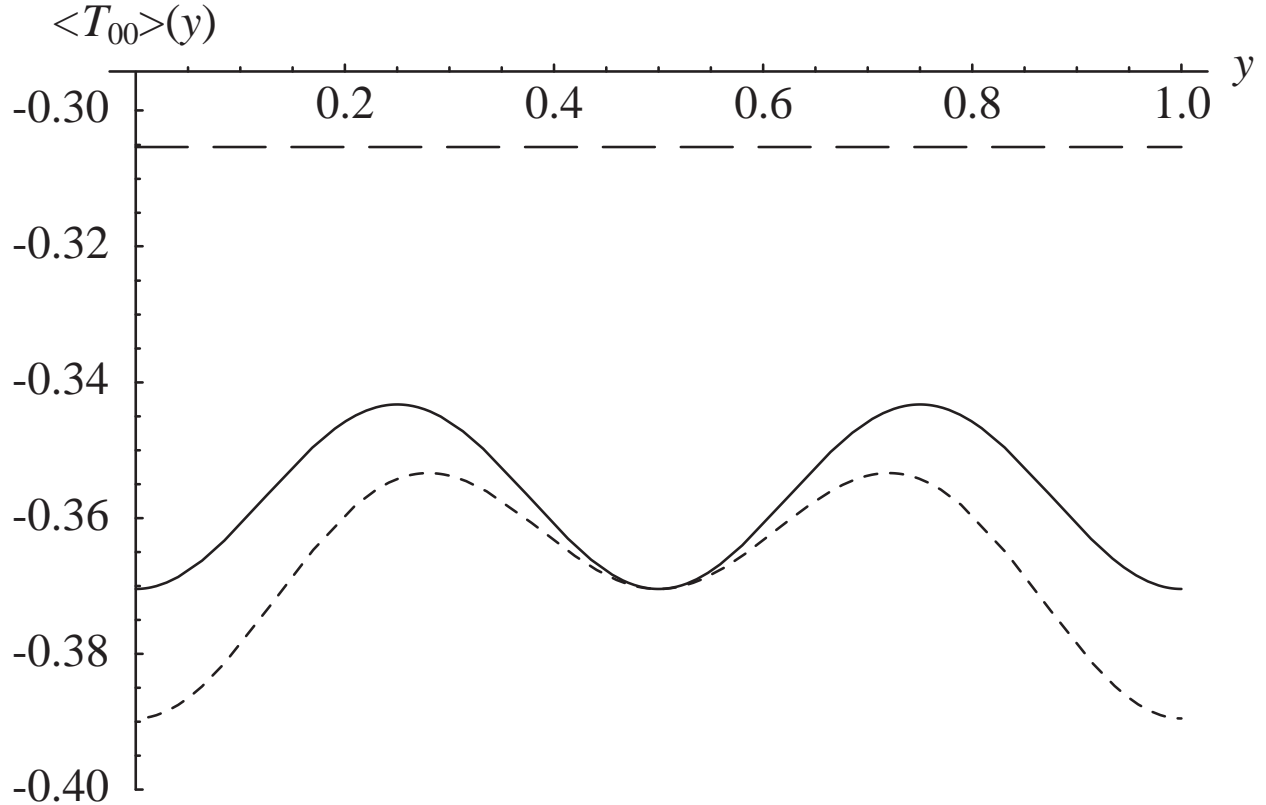


FIG. 4: Adding a flip: comparison of 2-Torus with Half-Turn (solid) and 2-Torus with Half-Turn and Flip (small dashed). Additionally, energy density of the plain 2-Torus (long dashed) is shown. The region is a single  $x = \text{const}$  and  $z = 0$  slice of the Fundamental Polyhedron.

### E. 2-Torus with Half-Turn and Flip ( $E_{15}$ )

We now combine all corkscrew and flipping motions to form a non-orientable manifold with interval

$$\sigma = \frac{1}{2} \{ -(t - \tilde{t})^2 + (x - \tilde{x} - n_x L_x)^2 + [y - (-1)^{n_x} \tilde{y} - n_y L_y]^2 + [z - (-1)^{n_x} (-1)^{n_y} \tilde{z}]^2 \}. \quad (25)$$

The resulting stress-energy tensor can be split into four separate summations corresponding to terms appearing in the stress-energy in simpler spaces. For example, we notice that if both  $n_x$  and  $n_y$  are even, we recover the interval for the 2-Torus. If both indices are odd, we

get the interval for the 2-Torus with Half-Turn. So we can build the stress-energy tensor as:

$$\begin{aligned} \langle T_{\mu\nu} \rangle_{E_{14}} = & \sum'_{n_x \text{ even}, n_y \text{ even}} [2\text{-Torus}] + \sum_{n_x \text{ odd}, n_y \text{ even}} [\text{Turn}(y, z)] \\ & + \sum_{n_x \text{ even}, n_y \text{ odd}} [\text{V-Flip}(z)] + \sum_{n_x \text{ odd}, n_y \text{ odd}} [\text{H-Flip}(y)]. \end{aligned} \quad (26)$$

The energy density in this space is shown in Figure 4.

## V. THREE CLOSED DIMENSIONS – TOROIDAL CROSS-SECTION

### A. 3-Torus ( $E_1$ )

The Fundamental Polyhedron is a rectangular box of width  $L_y$ , depth  $L_x$ , and height  $L_z$ . All pairs of opposite faces are identified. The interval is

$$\sigma = \frac{1}{2}[-(t - \tilde{t})^2 + (x - \tilde{x} - n_x L_x)^2 + (y - \tilde{y} - n_y L_y)^2 + (z - \tilde{z} - n_z L_z)^2]. \quad (27)$$

DeWitt, Hart, and Isham have shown that the resulting stress-energy is again constant, and it is repeated here:

$$\langle T_{\mu\nu} \rangle_{E_1} = \sum'_{n_x, n_y, n_z} [3\text{-Torus}], \quad (28)$$

where

$$\begin{aligned} [3\text{-Torus}] = & \frac{1}{2\pi^2} \frac{1}{(L_x^2 n_x^2 + L_y^2 n_y^2 + L_z^2 n_z^2)^3} \\ & \times (L_x^2 n_x^2 \text{diag}[-1, -3, 1, 1] + L_y^2 n_y^2 \text{diag}[-1, 1, -3, 1] \\ & + L_z^2 n_z^2 \text{diag}[-1, 1, 1, -3]). \end{aligned}$$

The energy density is more negative than its 2- and 1-Torus analogs. The corresponding calculation for a massive scalar field in the 3-Torus Space can be found in [3].

### B. Half-Turn Space ( $E_2$ )

When stacking boxes in the  $x$ -direction, we may flip in both  $y$ - and  $z$ -directions resulting in a rotation by  $180^\circ$  about the  $x$ -axis. The depth of the Fundamental Polyhedron is now

$2L_x$ , and the height and width remain the same. The interval in this orientable manifold is

$$\sigma = \frac{1}{2} \left\{ -(t - \tilde{t})^2 + (x - \tilde{x} - n_x L_x)^2 + [y - (-1)^{n_x} \tilde{y} - n_y L_y]^2 + [z - (-1)^{n_x} \tilde{z} - n_z L_z]^2 \right\}. \quad (29)$$

Proceeding by splitting into even and odd summations gives

$$\langle T_{\mu\nu} \rangle_{E_2} = \sum'_{\substack{n_x \text{ even} \\ n_y, n_z}} [\text{3-Torus}] + \sum_{\substack{n_x \text{ odd} \\ n_y, n_z}} [1/2\text{-Turn}(y, z)], \quad (30)$$

with

$$\begin{aligned} [1/2\text{-Turn}(y, z)] &= \frac{1}{6\pi^2} \frac{1}{[L_x^2 n_x^2 + (2y - L_y n_y)^2 + (2z - L_z n_z)^2]^3} \\ &\quad \times \left\{ L_x^2 n_x^2 \text{diag}[-5, -7, 1, 1] + (2y - L_y n_y)^2 \text{diag}[-1, 1, 1, -3] \right. \\ &\quad + (2z - L_z n_z)^2 \text{diag}[-1, 1, -3, 1] \\ &\quad \left. - 4(2y - L_y n_y)(2z - L_z n_z) (\delta_\mu^y \delta_\nu^z + \delta_\mu^z \delta_\nu^y) \right\}. \end{aligned}$$

Once again we see non-zero off-diagonal elements due to the corkscrew motion of this space. Since flipping occurs in both the  $y$ - and  $z$ -directions, we see in Figure 5 (a) periodic behavior in the vacuum energy density in both directions.

### C. Quarter-Turn Space ( $E_3$ )

If the width and height of the rectangular box are equal ( $L_y = L_z = L$ ), a quarter-turn, or  $90^\circ$ , corkscrew motion is allowed. This is another orientable manifold. The interval is now

$$\sigma = \frac{1}{2} \left\{ -(t - \tilde{t})^2 + (x - \tilde{x} - n_x L_x)^2 + \left[ y - \cos\left(\frac{n_x \pi}{2}\right) \tilde{y} + \sin\left(\frac{n_x \pi}{2}\right) \tilde{z} - n_y L \right]^2 + \left[ z - \sin\left(\frac{n_x \pi}{2}\right) \tilde{y} - \cos\left(\frac{n_x \pi}{2}\right) \tilde{z} - n_z L \right]^2 \right\}. \quad (31)$$

An explicit analytical expression for the stress-energy tensor in this space is omitted in favor of a numerical plot (see Figure 5 (b)). Since it takes four complete traversals in the  $x$ -direction to return to the original axes orientation, we find the frequency of periodicity of the energy density to be half that of the Half-Turn Space.

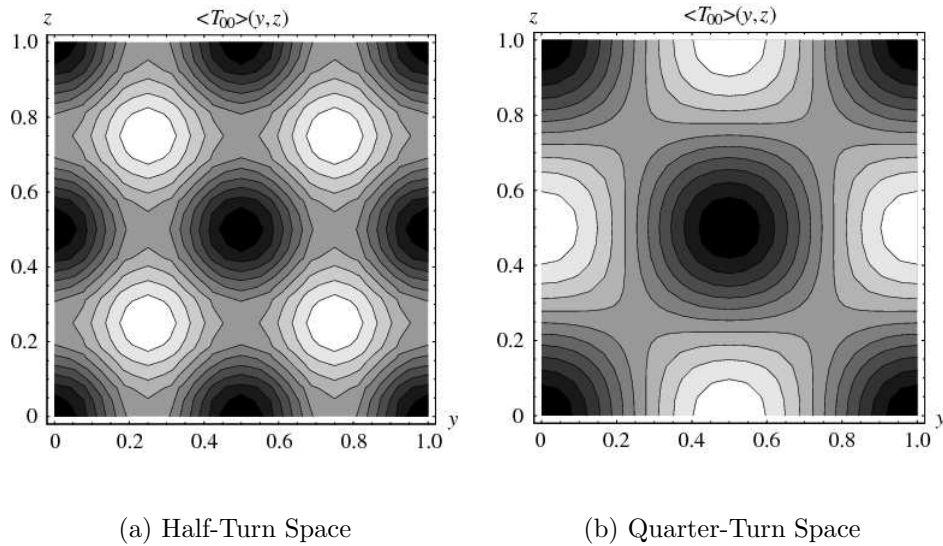


FIG. 5: Vacuum energy densities in the Half-Turn Space and the Quarter-Turn Space with  $L_x = L_y = L_z = L = 1$ . The regions are  $x = \text{const}$  slices of the Fundamental Polyhedron. Darker shading indicates more negative values.

#### D. Third-Turn Space ( $E_4$ )

It is possible for the  $y$ - and  $z$ -axes to rotate by  $120^\circ$  as we translate in the  $x$ -direction by  $L_x$ . In such a case, the Fundamental Polyhedron is a hexagonal prism. Within this space, each  $x = \text{const}$  slice will be a hexagonal torus. Let the distance between base points (the distance from one rectangular face to the opposite side) be  $L$ , and the height of each prism layer to be  $L_x$ . The depth of this Fundamental Polyhedron is thus  $3L_x$ . The spacetime remains orientable. The interval is now

$$\sigma = \frac{1}{2} \left\{ - (t - \tilde{t})^2 + (x - \tilde{x} - n_x L_x)^2 + \left[ y - \cos\left(\frac{2n_x \pi}{3}\right) \tilde{y} + \sin\left(\frac{2n_x \pi}{3}\right) \tilde{z} - n_y L - \frac{1}{2} n_z L \right]^2 + \left[ z - \sin\left(\frac{2n_x \pi}{3}\right) \tilde{y} - \cos\left(\frac{2n_x \pi}{3}\right) \tilde{z} - \frac{\sqrt{3}}{2} n_z L \right]^2 \right\}. \quad (32)$$

The numerical result is shown in Figure 6 (a). The energy density exhibits the hexagonal structure of the underlying topology.

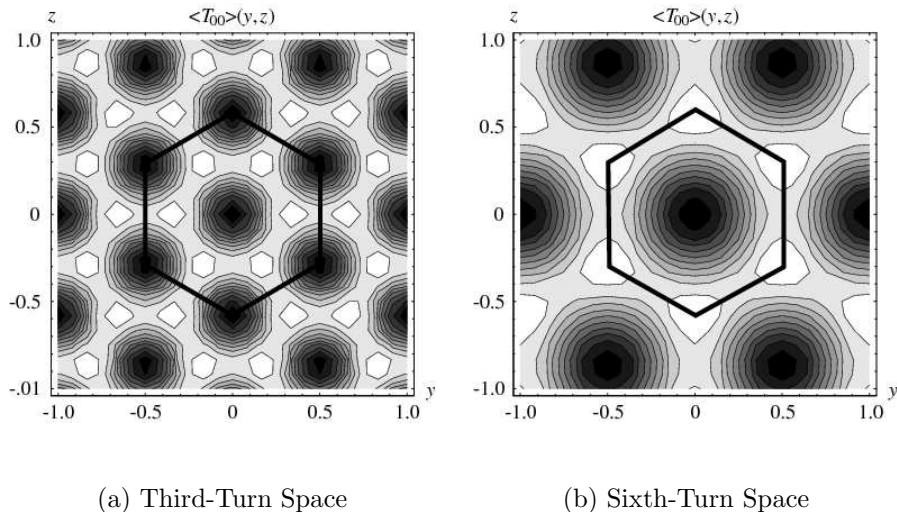


FIG. 6: Vacuum energy densities in the Third-Turn Space and the Sixth-Turn Space with  $L_x = L = 1$ . The heavy black line indicates the region of a  $x = \text{const}$  slice of the Fundamental Polyhedron.

### E. Sixth-Turn Space ( $E_5$ )

The hexagonal prism could be rotated by  $60^\circ$  when stacked in the  $x$ -direction. The Fundamental Polyhedron's depth is now  $6L_x$ . Once again, this is an orientable spacetime. The interval is thus

$$\sigma = \frac{1}{2} \left\{ - (t - \tilde{t})^2 + (x - \tilde{x} - n_x L_x)^2 + \left[ y - \cos\left(\frac{n_x \pi}{3}\right) \tilde{y} + \sin\left(\frac{n_x \pi}{3}\right) \tilde{z} - n_y L - \frac{1}{2} n_z L \right]^2 + \left[ z - \sin\left(\frac{n_x \pi}{3}\right) \tilde{y} - \cos\left(\frac{n_x \pi}{3}\right) \tilde{z} - \frac{\sqrt{3}}{2} n_z L \right]^2 \right\}. \quad (33)$$

Figure 6 (b) shows our numerical result.

## VI. HANTZSCHE-WENDT SPACE ( $E_6$ )

To generate the Hantzsche-Wendt manifold, imagine a rectangular box of sides  $L_x$ ,  $L_y$ , and  $L_z$  and three orthogonal, nonintersecting axes, each on a face of the box. When the box is translated along one of the axes by its length, a half-turn corkscrew motion about that axis is introduced [4]. The Fundamental Polyhedron of the Hantzsche-Wendt Space is



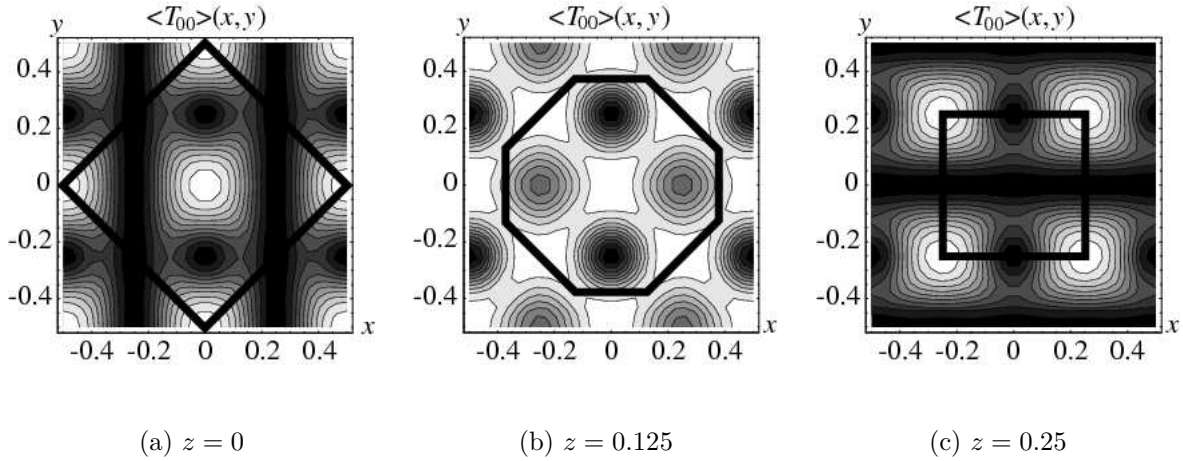


FIG. 7: Energy density in Hantzsche-Wendt Space. Shown are the three planes in the Fundamental Polyhedron, indicated by the heavy black line within each plot.

a rhombic dodecahedron which circumscribes the rectangular box. The Hantzsche-Wendt Space is an orientable manifold. The interval in this space is given by

$$\sigma = \frac{1}{2} \left\{ - (t - \tilde{t})^2 + \left[ x - (-1)^{n_b} (-1)^{n_c} \tilde{x} - (n_a + n_b) \frac{L_x}{2} \right]^2 + \left[ y - (-1)^{n_a} (-1)^{n_c} \tilde{y} - (n_b + n_c) \frac{L_y}{2} \right]^2 + \left[ z - (-1)^{n_a} (-1)^{n_b} \tilde{z} - (n_a + n_c) \frac{L_z}{2} \right]^2 \right\}, \quad (34)$$

where  $n_a$ ,  $n_b$ , and  $n_c$  are any integers.

The resulting energy density is a function of all three spatial dimensions. Shown in Figure 7 is slices of this space in the  $x-y$  plane at  $z = 0, 0.125, \text{ and } 0.25$ . This is identical to slices through the center of the Fundamental Polyhedron for the other two planes, as well.  $L_x$ ,  $L_y$ , and  $L_z$  have been set equal to 1.

## VII. THREE CLOSED DIMENSIONS – KLEIN BOTTLE CROSS-SECTION

To construct the Klein Spaces, start with a flat rectangular box of length  $L_x$ , width  $L_y$ , and height  $L_z$ . Glue the faces in the  $y$ - and  $z$ -directions in the usual way, but glue the faces in the  $x$ -direction with a flip in the  $y$ -direction. This flipping results in a glide reflection in the  $y$ -coordinate under translations in the  $x$ -direction. The resulting space is a Klein bottle

cross a circle ( $K^2 \times S^1$ ). While stacking the rectangles in the  $z$ -direction, a vertical flip (in the  $x$ -coordinate), horizontal flip (in the  $y$ -coordinate), or a half-turn (about the  $z$ -axis) could be introduced, yielding a total of four Klein Spaces. Because of the flipping motions, all of the Klein Spaces are non-orientable.

### A. Klein Space ( $E_7$ )

Klein spaces have many possible Fundamental Polyhedra. For simplicity, we will choose a rectangular box of length  $2L_y$ , width  $L_x/2$  and height  $L_z$ . Then, the interval in the basic Klein Space is given by

$$\sigma = \frac{1}{2} \{ -(t - \tilde{t})^2 + (x - \tilde{x} - n_x L_x/2)^2 + [y - (-1)^{n_x} \tilde{y} - 2n_y L_y]^2 + (z - \tilde{z} - n_z L_z)^2 \}. \quad (35)$$

The vacuum stress-energy tensor can be split into two summations over even and odd indices:

$$\langle T_{\mu\nu} \rangle_{E_7} = \sum'_{\substack{n_x \text{ even} \\ n_y, n_z}} [\text{Klein}] + \sum_{\substack{n_x \text{ odd} \\ n_y, n_z}} [\text{K-Flip}(y)], \quad (36)$$

where

$$\begin{aligned} [\text{Klein}] &= \frac{8}{\pi^2} \frac{1}{(L_x^2 n_x^2 + 16L_y^2 n_y^2 + 4L_z^2 n_z^2)^3} \\ &\times (L_x^2 n_x^2 \text{diag}[-1, -3, 1, 1] + 16L_y^2 n_y^2 \text{diag}[-1, 1, -3, 1] \\ &+ 4L_z^2 n_z^2 \text{diag}[-1, 1, 1, -3]) \end{aligned}$$

and

$$\begin{aligned} [\text{K-Flip}(y)] &= \frac{32}{3\pi^2} \frac{1}{[L_x^2 n_x^2 + 16(y - L_y n_y)^2 + 4L_z^2 n_z^2]^3} \\ &\times (L_x^2 n_x^2 \text{diag}[-1, -2, 0, 1] + 4L_z^2 n_z^2 \text{diag}[-1, 1, 0, -2]). \end{aligned}$$

The even summation over  $n_x$  produces a constant shift in the vacuum energy density similar to the 3-Torus case whereas the odd summation gives us a periodic  $y$ -dependence (see Figure 8).

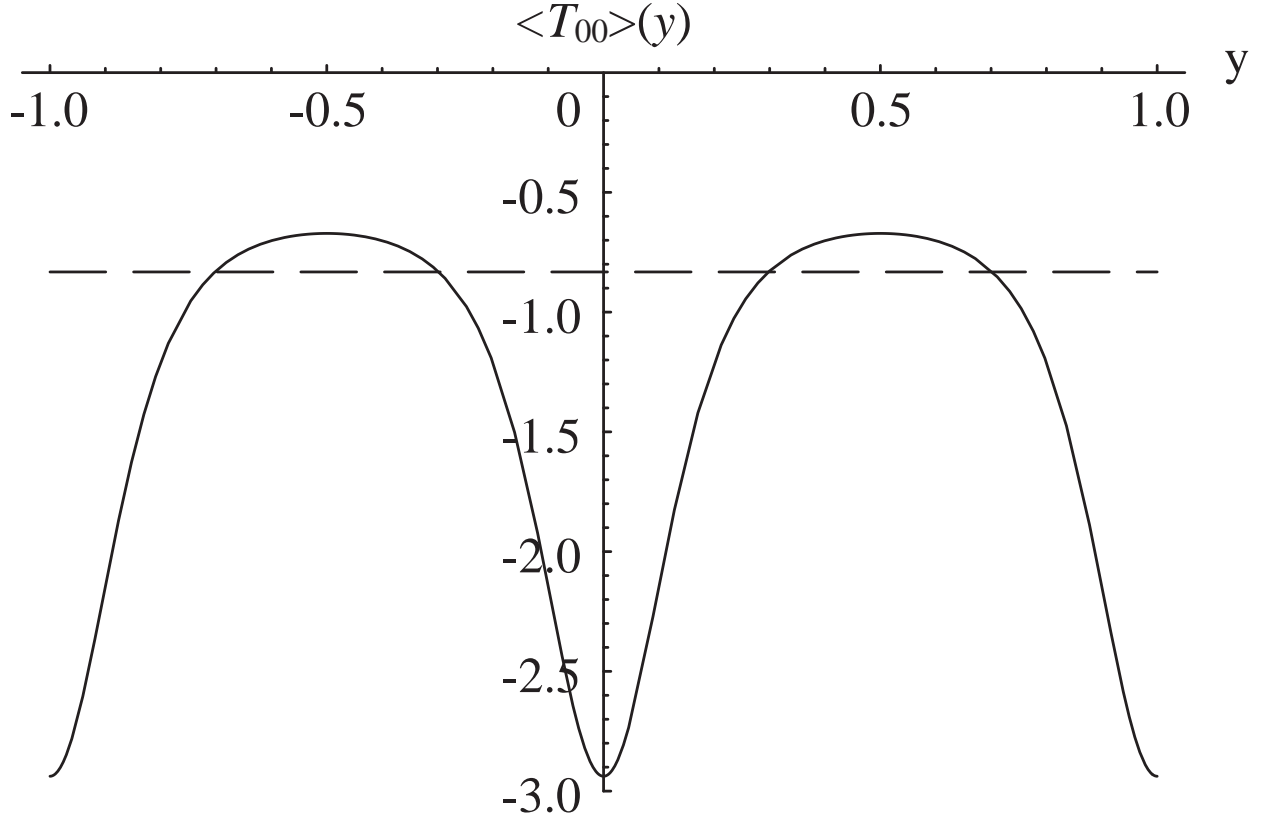


FIG. 8: Comparing the vacuum energy densities in 3-Torus Space (dashed line) and Klein Space (solid lines), with  $L_x = L_y = L_z = 1$ . The region is a single  $z = \text{const}$  and  $x = 0$  slice of the Fundamental Polyhedra. Note that we are showing two Fundamental Polyhedron of the 3-Torus Space, to aid in comparison.

### B. Klein Space with Horizontal Flip ( $E_8$ )

When stacking rectangular Fundamental Polyhedra in the  $z$ -direction, a horizontal flip in the  $y$ -direction can be introduced, yielding an interval of

$$\sigma = \frac{1}{2} \{ -(t - \tilde{t})^2 + (x - \tilde{x} - n_x L_x / 2)^2 + [y - (-1)^{n_x} (-1)^{n_z} \tilde{y} - 2n_y L_y]^2 + (z - \tilde{z} - n_z L_z)^2 \}. \quad (37)$$

By carefully examining this interval, and arranging the summations correctly, we can get the exact same result as for the simple Klein space. We may write

$$\langle T_{\mu\nu} \rangle_{E_8} = \sum'_{\substack{n_x \text{ and } n_z \text{ even} \\ \text{or} \\ n_x \text{ and } n_z \text{ odd} \\ n_y}} [\text{Klein}] + \sum_{\substack{n_x \text{ even, } n_z \text{ odd} \\ \text{or} \\ n_x \text{ odd, } n_z \text{ even} \\ n_y}} [\text{K-Flip}(y)]. \quad (38)$$

### C. Klein Space with Vertical Flip ( $E_9$ )

Alternatively, we may flip in the vertical direction,  $x$ , as we translate in the  $z$ -direction:

$$\sigma = \frac{1}{2} \left\{ -(t - \tilde{t})^2 + [x - (-1)^{n_z} \tilde{x} - n_x L_x / 2]^2 + [y - (-1)^{n_x} \tilde{y} - 2n_y L_y]^2 + (z - \tilde{z} - n_z L_z)^2 \right\}. \quad (39)$$

Each of four possible combinations of  $n_x$  and  $n_z$  gives a different functional form:

$$\begin{aligned} \langle T_{\mu\nu} \rangle_{E_9} = & \sum'_{\substack{n_x \text{ even} \\ n_y \text{ even} \\ n_z \text{ even}}} [\text{Klein}] + \sum_{\substack{n_x \text{ odd} \\ n_y \text{ even} \\ n_z \text{ even}}} [\text{K-Flip}(y)] \\ & + \sum_{\substack{n_x \text{ even} \\ n_y \text{ odd} \\ n_z \text{ odd}}} [\text{K-V-Flip}(x)] \sum_{\substack{n_x \text{ odd} \\ n_y \text{ odd} \\ n_z \text{ odd}}} [\text{K-Turn}(x, y)], \end{aligned} \quad (40)$$

with

$$\begin{aligned} [\text{K-V-Flip}(x)] = & \frac{128}{3\pi^2} \frac{1}{[(4x - L_x n_x)^2 + 16L_y^2 n_y^2 + 4L_z^2 n_z^2]^3} \\ & \times (L_x^2 n_x^2 \text{diag}[-1, 0, 1, -2] + 4L_y^2 n_y^2 \text{diag}[-1, 0, -2, 1]) \end{aligned}$$

and

$$\begin{aligned} [\text{K-Turn}(x, y)] = & \frac{8}{3\pi^2} \frac{1}{[(4x - L_x n_x)^2 + 16(y - L_y n_y)^2 + 4L_z^2 n_z^2]^3} \\ & \times \left\{ (4x - L_x n_x)^2 \text{diag}[-1, 1, -3, 1] \right. \\ & + 16(y - L_y n_y)^2 \text{diag}[-1, -3, 1, 1] + 4L_z^2 n_z^2 \text{diag}[-5, 1, 1, -7] \\ & \left. + 16(4x - L_x n_x)(y - L_y n_y) (\delta_\mu^x \delta_\nu^y + \delta_\mu^y \delta_\nu^x) \right\}. \end{aligned}$$

### D. Klein Space with Half-Turn ( $E_{10}$ )

The last space is the Klein Space with Half-Turn in which a corkscrew motion of  $180^\circ$  about the  $z$ -axis is introduced, generating an interval of

$$\sigma = \frac{1}{2} \left\{ -(t - \tilde{t})^2 + [x - (-1)^{n_z} \tilde{x} - n_x L_x / 2]^2 + [y - (-1)^{n_x} (-1)^{n_z} \tilde{y} - 2n_y L_y]^2 + (z - \tilde{z} - n_z L_z)^2 \right\}. \quad (41)$$

Interestingly,  $\langle T_{\mu\nu} \rangle$  contains the same four summations as those for the Klein Space with Vertical Flip except that the indices for the last two summations are exchanged.

$$\begin{aligned} \langle T_{\mu\nu} \rangle_{E_{10}} = & \sum'_{\substack{n_x \text{ even} \\ n_y \text{ even} \\ n_z \text{ even}}} [\text{Klein}] + \sum_{\substack{n_x \text{ odd} \\ n_y \text{ even} \\ n_z \text{ even}}} [\text{K-Flip}(y)] \\ & + \sum_{\substack{n_x \text{ odd} \\ n_y \text{ odd} \\ n_z \text{ odd}}} [\text{K-V-Flip}(x)] + \sum_{\substack{n_x \text{ even} \\ n_y \text{ odd} \\ n_z \text{ odd}}} [\text{K-Turn}(x, y)]. \end{aligned} \quad (42)$$

The vacuum energy densities in Klein Spaces with Horizontal Flip, Vertical Flip, and Half-Turn deviate very little from that in the simple Klein Space. Flips and turns introduce only small modulations in the vacuum energy density.

### VIII. TOPOLOGICAL EFFECTS ON THE VACUUM ENERGY DENSITY

Despite many differences among the results described above, there are quite a few similarities. Every vacuum energy density calculated is negative relative to the value in the simply-connected Minkowski space. All of the results are dependent on the size of the Fundamental Polyhedron. Specifically, the stress-energies of all the spaces are proportional to the inverse-fourth power of the length of the Fundamental Polyhedron. Thus, as the size of the Fundamental Polyhedra increases the vacuum energy density approaches zero. This is because the scalar field is allowed to have more modes, pushing the value of vacuum density upward to zero.

By closing a single dimension, the vacuum energy density shifts downward by a constant. As we move to the 2-Torus and 3-Torus, the energy density shifts even further. Closing more dimensions reduces the number of modes available to the quantum field (as noted by DeWitt and others [1]). The wavelength must have discrete values not only in the  $x$ -direction but also in the  $y$ - and  $z$ -directions. This shift in the energy density is always a constant throughout the universe and never position-dependent.

The vacuum energy density also reflects the symmetries of the underlying Fundamental Polyhedron. The densities of 1/4-Turn and 1/2-Turn spaces are repeating patterns of rectangular grids, like squares on a checkerboard. However, the densities of 1/6-Turn and 1/3-Turn spaces are repeating hexagon patterns, mirroring how the Fundamental Polyhedron is tiled.

Moreover, the value of the vacuum energy density is dependent on the cross section of

Tiling	Energy Density
1-Torus	-0.11
2-Torus	-0.31
Rectangular 3-Torus	-0.83
Hexagonal prism	-0.99
Klein space	-2.39
Hantzsche-Wendt Space	-0.32

TABLE I: Possible tilings of three-dimensional space and their associated shift in vacuum energy density relative to Euclidean space. For these calculations,  $L_x = L_y = L_z = L = 1$  in all cases, only the constant, position-independent terms are calculated.

the Fundamental Polyhedron. For the Klein Spaces, the cross section of the Fundamental Polyhedron is a Klein bottle, resulting in a lower energy density than the 3-Torus spaces with the toroidal cross section. Likewise, the hexagonal torus of Third- and Sixth-Turn Spaces reduces the energy density below the Minkowski level, but not to the extent of the Klein bottle cross section. Table I summarizes shifts in the constant, position-independent part of the energy density due to various cross sections of the Fundamental Polyhedron.

Positional dependence of the stress-energy tensor appears if we add flipping or corkscrew motions when gluing faces of the Fundamental Polyhedra. When a dimension undergoes a reflection or turn, the stress-energy tensor becomes dependent on that direction. For example, in the Third-Turn Space, we rotate the  $y$ - and  $z$ -coordinates, so  $\langle T_{\mu\nu} \rangle$  depends on  $y$  and  $z$  but is still independent of  $x$ . If the flipped dimension is closed, as the universe is traversed in that direction, the energy density well is encountered again and again at a constant interval.

If the flipped dimension is open, a single well appears in the energy density, and translational symmetry is broken. For example, consider Figure 2, which is the plot of the energy density in the 1-Torus with Flip. The energy density reaches a minimum where  $y = 0$ . The vacuum energy density will be symmetric about this plane. If we were traveling in this universe in the  $y$  direction, we would eventually encounter this location where the energy density is at a minimum. Figure 3 compares effects of flips in different directions in 2-Torus spaces. In the 2-Torus with Vertical Flip, the flip occurs in an open dimension ( $z$ ) resulting

in a single well in the energy density at  $z = 0$ . In the 2-Torus with Horizontal Flip, we have periodic wells in the  $y$ -direction because the flip occurs in a closed dimension ( $y$ ).

Direct comparisons of vacuum energy density plots reveal many interesting features. For example, Figure 4 shows the results of adding an additional flip to the 2-Torus with Half-Turn. While they have the same value in the center of the Fundamental Polyhedron, the flipping causes the energy density to reach a lower value on the boundary of the Fundamental Polyhedron.

Similarly, we notice the effects of various rotational angles by examining Figure 9. This plot features the corkscrew motions on the 3-Torii. The strongest difference in energy densities is due to switching from rectangular to hexagonal torus of the Fundamental Polyhedron, while increased rotations (i.e. from  $90^\circ$  to  $180^\circ$  rotations) do not change the average value, but instead change the periodicity.

Our calculations in various Klein Spaces show that the amplitude of the periodic wells in the vacuum energy density, introduced by switching from the rectangular cross section to the Klein bottle cross section, is much larger than the amplitude of the amplitude of the modulations due to flips and turns.

## IX. CONCLUSION

We have discovered that the vacuum expectation value of the stress-energy tensor in non-trivial manifolds exhibits the following qualitative behaviors : (1) increasing the number of closed dimensions further lowers the vacuum energy density relative to the zero value of the simply-connected Minkowski space, (2) the spatial pattern of the vacuum energy density follows the shape of the chosen Fundamental Polyhedron, (3) if a flip is added in a particular direction, then there will be a positional dependence in that particular direction, (4) if a turn is introduced, the stress-energy tensor will be dependent on the coordinates in the plane perpendicular to the rotational axis and will contain off-diagonal elements, and (5) the chosen cross section of the Fundamental Polyhedron greatly effects the relative vacuum energy densities, whereas flips and turns introduce only a minor position-dependent shift.

---

[1] B. S. Dewitt, C. F. Hart, and C. J. Isham, *Physica* **96A**, 197 (1979).

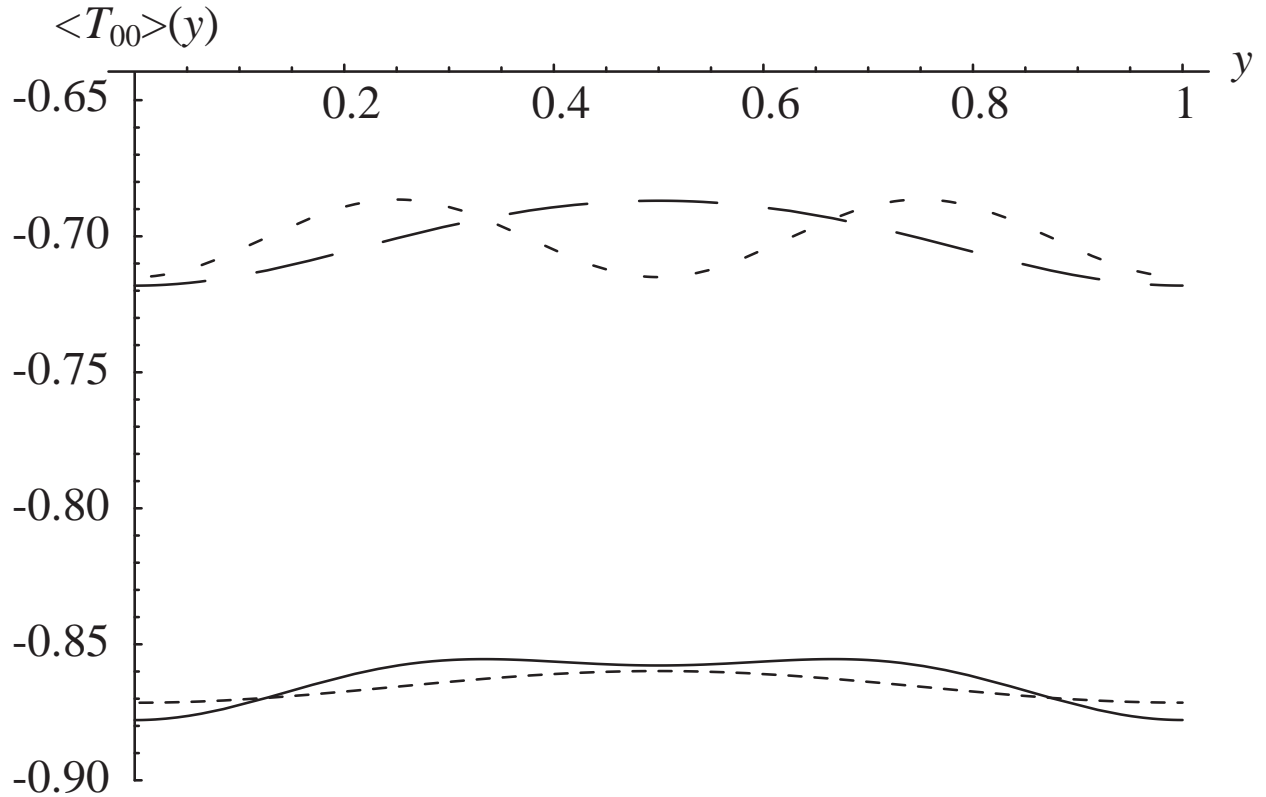


FIG. 9: Comparison of 3-Torii with different angles of rotation. Shown are: Half-Turn Space (short dash, long gap), Quarter-Turn Space (long dash), Third-Turn Space (solid), and Sixth-Turn Space (short dash, short gap). The region is a single  $x = \text{const}$  and  $z = 0$  region of the Fundamental Polyhedron. Note that for the Third- and Sixth-Turn Spaces, the energy density is shifted by one half-length of the Fundamental Polyhedron, to aid in comparison.

- [2] A. Riazuelo, J. Weeks, J.-P. Uzan, R. Lehoucq, and J.-P. Luminet, Phys. Rev. D **69**, 103518 (2004).
- [3] T. Tanaka and W. A. Hiscock, Phys. Rev. D **52**, 4503 (1995).
- [4] J. Levin, Phys. Rep. **365**, 251 (2002).
- [5] N. D. Birrell and P. C. W. Davies, *Quantum fields in curved space* (Cambridge University Press, 1982).
- [6] N. J. Cornish, D. N. Spergel, G. D. Starkman, and E. Komatsu, Phys. Rev. Lett. **92**, 201302 (2004).
- [7] M. J. Reboucas and G. I. Gomero, Braz. J. Phys. **34**, 1358 (2004).
- [8] D. Müller, H. Fagundes, and R. Opher, Phys. Rev. D **66**, 083507 (2002).



[9] J. R. Weeks, *The Shape of Space* (Marcel Dekker, Inc., 2002).